



Short-term estimation of beach sedimentation pattern in the mixed-energy environment at Digha coast, India

Subrata Jana¹

Received: 24 April 2021 / Revised: 14 November 2021 / Accepted: 15 November 2021 / Published online: 25 November 2021
© The Author(s), under exclusive licence to Springer Nature Switzerland AG 2021

Abstract

The short-term, long-term and seasonal hydro-morphodynamics and associated sedimentation patterns need to assess in prior aspects concerning the beach nourishment in the erosive coast. However, only the long-term and seasonal beach sedimentation patterns have been studied considering the monsoon phases in the Digha coast. In this study, the field investigation was conducted for 15 days during the 10–24 March 2018 to understand the morphodynamics, hydrodynamics and sedimentation pattern in the meso-tidal and wave-dominated mixed-energy environment in three different beach zones according to tide level. Beach bathymetry survey, wave hydrodynamic measurements and sediment sampling was done coupling with the empirical formulation of data through the geo-statistical methods. The high, moderate and low level of wave dynamics are observed in zone 3, 1 and 2, respectively. The resultant depth of closure varies from 0.94 to 1.28 m according to the fluctuating tide level. Along the four cross-profiles in-between the low-tide level (LTL) and high-tide level (HTL), the sedimentation pattern reveals the accretion in zone 1 (~0.81 cm) and 3 (~0.11 cm), while meager erosion in zone 2 (~0.02 cm). Such type of sedimentation pattern synchronizes with the net sediment volume detained by swash and backwash, which indicates a surplus volume in zone 1 (~50.09 gm) and 2 (~132.36 gm), and deficit (~52.62 gm) in zone 3.

Keywords Wave hydrodynamics · Mixed-energy environment · Depth of closure · Sedimentation pattern · Beach morphodynamics · Digha coast

1 Introduction

The terrestrial (rivers), coastal (tides, currents, waves, storm surges) and atmospheric (wind) agents are advent to coast and frequently interact together to reform distinct morphological features in-between the extreme high-tide level (HTL) and low-tide level (LTL) in the beach (Masselink & Short, 1993; Short & Wright, 2018). Tide is the most important hydrodynamic regulator, responsible for the positional shifting of wave actions and resultant morphodynamics (Butt & Russell, 2000; Sreenivasulu et al., 2017; Wright & Short, 1984). The beach morphological configuration depends on the sediment entrainment, transport and deposition under the reworking nature and magnitude of wave hydrodynamics

like wave height, length and energies coupled with currents and tides (Jackson et al., 2017; Kaliraj et al., 2017; Komar, 2018; Ramakrishnan et al., 2018). The nature and dynamism of micro-morphological features depend on the breaking wave height, wave energy, wave approaching angle and wave run-up length, including existing beach morphology (Ariffin et al., 2019; Carter, 2013). The utmost micro-landform modifies within the surf zone due to repeated wave hydrodynamics (Brinkkemper et al., 2018) in fluctuating tide levels (Chempalayil et al., 2014; Masselink & Hegge, 1995; Mujal-Colilles et al., 2019). During the high tide at the spring phase, the upper beach-face synchronizes plunging or surging breakers resulted in an enhanced reflective surf zone, whereas, at low tide only spilling breakers operating within a wide dissipative surf zone (Short & Wright, 2018).

The characterization of grain size distribution pattern is an important evidence of sediment entrainment, transportation and depositional environment influenced by hydrodynamic temperament within the intertidal beach stretch (Folk & Ward, 1957; Joevivek & Chandrasekar, 2019; Joevivek et al., 2018; Masselink et al., 2007). The wave hydrodynamic

Communicated by M. Michaelovitch de Mahiques.

✉ Subrata Jana
subrata.vumid@gmail.com

¹ Department of Geography, Belda College, Paschim Medinipur, Belda, India

nature and depth of closure (closeout depth) changed according to tide level (Birkemeier, 1985; Hallermeier, 1981; Morang & Birkemeier, 2005). The long-shore and cross-shore currents and littoral cell circulation systems have a contribution to the sediment budget (surplus or deficit) within the beach (Maiti & Bhattacharya, 2009).

At present, the beach as well as shoreline erosion, and this erosion management is a prime aspect in dynamic wave actions. It is desired to protect the shoreline and beach erosion in the viewpoint of changes in sea level and immense population pressure in the coastal zone. In this aspect, various types of erosion protection structures are constructed along the shoreline throughout the world (Jayappa et al., 2003; Williams et al., 2018). The estimations of seasonal beach erosion and accretion rate and associated hydrodynamics are usually adopted around the world. Generally, in the tropical monsoon-dominated coastal areas, pre- and post-monsoon beach morphological studies are also taken under consideration on a seasonal basis to understand the dynamic behaviour of the beach. However, the study of short-term or diurnal hydrodynamic behaviour and sedimentation pattern is also significant in the wake of proper adaptation of site-specific erosion protection strategies and beach nourishment. Concerning all those aspects, coastal areas draw the attention of every researcher, scientist, engineer and administrator throughout the world.

The present study has been carried out over the sandy beach stretch in Digha owing to all those aspects. The morphodynamic diversities have been considered with added effects of wave hydrodynamic, fluctuating tide levels and sediment distribution. In every pulse of time, hydraulic motion acts on sediment particles within the surf zone, accordingly particles are entrained, transported and deposited to convey a significant morphological change depending on the sediment grain size (Belliard et al., 2019). During the LTL, different micro-morphological features are observed within the beach. The estimation of such sort of morphological features is rather difficult unless adopting the very high-resolution airborne image and intensive field study (Belliard et al., 2019). Since the 1970s, plenty of works have been done in and around the Digha coast concerning the beach morphology and erosion using the seasonal beach profiling by leveling survey and remote sensing images (Adhikari et al., 2016; Bhattacharya et al., 2003; Chakrabarti, 1991; Jana & Bhattacharya, 2013; Maiti & Bhattacharya, 2009; Purkait & Majumdar, 2014; Purkait et al., 2017). However, the combined effects of wave hydrodynamic and beach sediments were not considered in the earlier assessment of beach morphodynamics. The real processes and responding sedimentation pattern and morphodynamics cannot be justified properly unless the study of beach morphology, sedimentology and hydraulics are in a conjoin form. Therefore, the present study aims to understand the short-term diversities

of sedimentation patterns and morphodynamics associated with spatio-temporal variation of wave hydrodynamics in diverse tide conditions over the Digha beach stretch.

2 Materials and methods

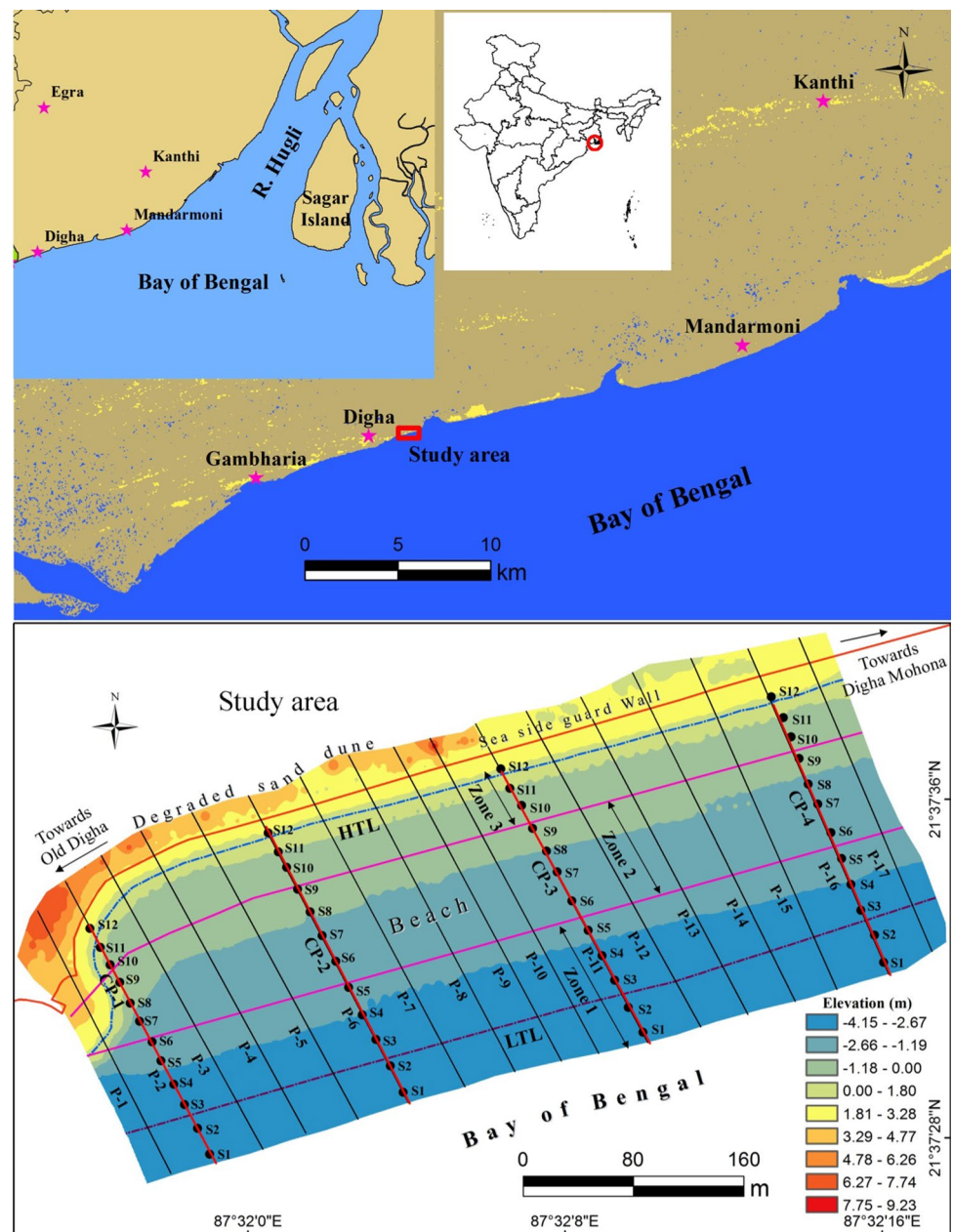
2.1 Study area

The Digha coast is situated within the meso-tide range (2–4 m) characterized by mean annual significant wave height of 0.6–1.2 m, average wind speed of 9.27 m/s (Patra & Bhaskaran, 2017) and about 5–6 cyclone strikes in every year (Mondal, 2021; Singh et al., 2001). Moreover, the negative shoreline shifting (–19.98 m/year) is observed in the Digha coastal stretch (Maiti & Bhattacharya, 2009). In this condition, the present study was conducted along the 700 m long beach stretch in the northern part of Digha coast between Old Digha and Digha Mohona (Champa river mouth) covering 0.16 km² area which is extended between 21° 37' 26.63" N to 21° 37' 39.91" N and 87° 31' 53.85" E to 87° 32' 17.56" E (Fig. 1). The studied beach stretch is highly erosive in comparison to the other parts of the Digha coast (around New Digha). Initially, along the erosive shoreline, the management policies were taken repeatedly often employing wooden fencing and laterite boulder filling. In spite of erosion protection structures, the shoreline retreat rate is gradually accelerated which is enforced to construct different hard defensive structures along the shoreline (Bhattacharya et al., 2003). However, in every stage, positions of the defensive structure were shifted towards the land in wake of land (dune) erosion. These hard defensive structures convey to an erosive beach from the dissipative or intermediate beach, as observed in the Old Digha section. As a result, the lateral erosion rate is reduced to some extent, but the vertical erosion rate is accelerated in recent times. Very recently in 2016, concreted wave dissipation blocks (with 5–9 stage wave breakers) and seawall has been constructed along the shoreline to shield the erosion. In 1997, a similar structure was constructed along the shoreline (600 m) in Old Digha (besides the present study area). But this structure ensures a reflective wave (plunging to collapsing wave breaking) from the dissipative wave environment (spilling wave breaking) coupled with a higher rate of beach erosion in terms of beach lowering. Therefore, such type of structure can only be able to protect the lateral erosion and shoreline retreat but accelerates the beach lowering.

2.2 Database

In this study, the database comprises two sub-sections: (i) 15 days field observations during the last to first quarter lunar phase (10–24 March 2018) on beach morphology,

Fig. 1 The study area at the nearshore part of the Digha coastal stretch (between Old Digha and Digha Mohona) depicts the elevation differences within the beach-dune transition zone, over which seventeen cross-profiles (P-1 to P-17) are demarcated. Hydrodynamic measurements were carried out in the three micro-zones (zone 1, 2, and 3) between the HTL and beyond the LTL. Along the four distinct cross-profiles (CP-1 to CP-4) the repetitive profiling survey was conducted by total station, and twelve sediment samples (S1 to S12) were collected from each of these four cross-profiles



hydrodynamics and sedimentological parameters, and (ii) primary data analysis through geographic information system (GIS), equation-based hydrodynamic computation and empirical models based on statistics.

2.2.1 Total station survey

On 10 March 2018, the bathymetry survey was carried out over the entire beach stretch (0.16 km^2) through the Total Station (Leica FlexLine TS07) in-between the degraded dune (landward) and far seaward side beyond the LTL. The instrument was placed over the newly constructed seaside guard-wall cum road (marine drive road) (Fig. 2a) at an

elevation of $\sim 3.25 \text{ m}$, based on the tidal benchmark after considering the mean lower low tide water level at that site. The easting-northing-height (ENH) was assigned as 555,350 (E), 2,391,637 (N) and 3.213 m (H) considering the real-time kinematic global positioning systems (RTK-GPS) based coordinate. Within the study area, total 36,756 points ($\sim 2 \text{ m}$ spatial interval) were taken with the accuracy of 1 mm (horizontal) and 0.1 mgon or 0.1" (vertical angle) in the normal weather condition. Depending on the topographic (elevation) differences of undulated and relatively flat areas, the reflectors were placed either nearby or in a secluded position. At every point, distance and angles were recorded in the memory of Total Station concerning

Fig. 2 Data collection (a) through Total station survey; measurements of (b) breaking wave height, (c) wavelength and frequency, and (d) wind speed; and collection of (e) sediment sample from the beach (f) and sediment volume from successive swash and backwash in different aspects of beach morphology, hydrodynamics and sedimentology



the referenced ENH. Furthermore, the elevations of all successive surveyed points were automatically calculated and recorded by the internal processor of the Total Station. The entire data was transferred into the GIS environment (ArcGIS v.10.4) according to the X , Y and Z , correspondingly assigning with easting, northing and height/elevation, respectively. This data was projected in Universal Transverse Mercator (UTM) coordinate system based on the 45 N zone and world geodetic survey 1984 (WGS 1984) datum. After converting the data file into shapefile (.shp) format, the inverse distance weighting (IDW) raster interpolation method was applied (with 0.1 m cell size) on elevation data. Finally, the very high-resolution (0.1 m) digital elevation model (DEM) was created. The beach elevation, slope, micro-morphological features and cross-profiles were delineated from the DEM. The Total Station survey was also conducted for three days on 19th, 20th and 21st March 2020 (at Waxing Crescent phase) for the profiling survey at 0.5 m interval along the four distinct cross-profiles (~218 m extents in-between HTL and beyond the LTL) of CP-1, CP-2, CP-3, and CP-4 (Fig. 1) to estimate the short-term sedimentation pattern.

2.2.2 Measurement of hydrodynamic parameters

Considering the morphological diversities the entire beach stretch was segmented into three distinct zones (zone 1, 2 and 3). The hydrodynamic parameters were recorded (Table 1) in three distinct zones i.e. the relatively steeper beach section near the LTL (zone 1) and HTL (zone 3), and in the relatively gentle beach section (zone 2) in-between the two steeper beach sections of zone 1 and 3. Data were taken at three different events (1st, 2nd and 3rd event) during the high-tide (rising stage, nearly at -1 m elevation zone), at high-tide (nearly at 1 m elevation zone), and low-tide (falling stage, at -3 m elevation zone) conditions in every day of the study period. At each event, hydrodynamic data of 225 simultaneous observations were recorded concerning the measurement of wave parameters with the effort of four groups of active students (Fig. 2b, c). Therefore, 10,125 hydrodynamic observation data were collected within 15 days of measurement. The detained sediment by every swash and backwash (1 m width of successive waves) (Fig. 2f) were also collected by the handmade plastic bag (1 m \times 1 m diameter) for a continuous 1 h period during

Table 1 Inconsistency of wind and wave parameters during the study period within the Old Digha-Digha Mohona beach stretch

Zone	Variable	Wind Speed (m/s)	Dominant wind direction	Wave height (m)		Wave-length (m)	Water depth (m)	Surf-zone width (m)	Wave run-up length (m)		Wave period (s)	Longshore current velocity (m/s)	Angle of wave approach (°) based on magnetic north			
				Crest	Trough				Average	Amplitude				Breaking		
1	Maximum	2.05	S-SSE	1.70	0.85	1.03	0.52	1.60	30.30	2.04	36.23	17.53	15.33	9.14	0.59	81.00
	Minimum	0.70	(163°)	0.95	0.64	0.30	0.15	0.88	7.70	1.28	21.14	8.32	6.12	6.40	0.24	64.00
	Average	1.31		1.30	0.73	0.57	0.29	1.28	13.38	1.66	23.26	12.51	8.24	7.13	0.38	72.43
2	Maximum	1.70	SE-SSE	1.61	0.73	0.79	0.40	1.52	49.60	1.94	64.35	23.03	21.31	10.50	0.41	88.00
	Minimum	0.50	(146°)	0.75	0.50	0.25	0.13	0.51	17.56	1.28	35.13	13.15	11.03	6.80	0.20	71.00
	Average	0.97		0.95	0.57	0.50	0.25	1.01	22.14	1.67	41.17	17.35	14.76	9.12	0.26	77.31
3	Maximum	3.63	SE (145°)	1.54	0.90	1.10	0.55	2.25	29.03	1.97	41.26	16.15	12.06	7.54	0.23	80.00
	Minimum	2.50		0.74	0.45	0.30	0.19	0.55	10.12	0.97	16.12	6.34	3.01	4.12	0.13	68.00
	Average	3.16		1.19	0.70	0.59	0.29	1.31	12.77	1.57	20.35	8.15	5.16	5.41	0.18	73.99

Measurements of wave parameters were conducted in three different events during 10–24 March 2018, during 9:30:00.00 to 9:49:25.71 h (1st event), 10:45:00.00 to 11:04:25.71 h (2nd event) and 1:00 to 1:19:25.71 h (3rd event) on every day at zone 1: relatively steeper beach section (near the LTL), zone 2: relatively gentle beach section (between zone 1 and 3), and zone 3: relatively steeper beach section (near the HTL). Here, only the summary of 35 observations from each event is represented. The observation events are simultaneously conducted during high-tide (rising and falling), extreme high-tide and low-tide (falling and rising) conditions

each event. During the hydrodynamic measurements, the wind speeds were simultaneously recorded by an anemometer (Fig. 2d). Based on Laing (1998), the basic theoretical concept of wave hydrodynamic measurements was adopted. The height of wave crests, troughs and wave breaking were measured using the measuring staff. Similarly, the wavelength, swash and backwash run-up length and surf zone width were measured through the measuring tape by four groups of students according to the wave approaches sites. The angle of wave approach was measured by the prismatic compass (in relation to magnetic north). The wave period was estimated considering the 'n' number of successive waves passing through a fixed site (fixed by ranging rod) at a fixed time (t) using a digital stopwatch. The longshore/shore-normal current velocity was calculated from the travelling distance and time of the wooden buoyant ball from 2 m distance ahead of the breaker point (Jayakumar et al., 2004). Other wave parameters were estimated using the different wave hydrodynamic equations.

2.2.3 Sediment sample collection and laboratory analysis

Surface sediment samples (~200 gm per sample) were collected across the beach stretch (Masselink et al., 2007) at a spatial interval of ~15 m depending on the morphological diversities. A total of 48 sediment samples, 12 (S1–S12) from each cross-profile of CP-1, 2, 3 and 4 (Fig. 1) as set-1, 2, 3 and 4 were collected, respectively (Fig. 2e). Among these 48 samples, 42%, 33%, and 25% of sediment samples were collected from zone 1, 2, and 3 (Fig. 1), respectively. The sieving method was employed for grain size analysis (Blatt et al., 1980) using the mechanical sieve shaker (for 15 min) with a quarter phi (0.25 ϕ) interval of sieves. Therefore, 13 sieves were used (with top and pan) ranging from 1.0 ϕ (500 μm) to 4.0 ϕ (63 μm) apertures following the United States Geological Survey (USGS) standard. The sediment grains retained in each size fraction by individual sieve were recorded (in gm) using a digital balance meter for further analysis adopting the recognized statistical methods in GRADISTAT (Blott & Pye, 2001). Moreover, volumes of detained sediment (weight in gm) of swash and backwash were estimated to assess the erosion and accretion trends in diverse hydrodynamic conditions in the different zones.

2.3 Data analysis

2.3.1 Digital elevation model based beach morphology evaluation

Different beach morphological features were extracted from the DEM. The elevation, contour pattern and slope (β) were analyzed (Figs. 1, 3) using ArcGIS 10.4 software. 17 cross-profiles (P-1 to P-17) were compiled from the land towards

the sea (Fig. 1). The geometric properties of uniform spacing cusps-horns and ridge-runnels were measured on the field and also extracted from the DEM. The 3-dimensional forms of those features were validated through the root mean square error (RMSE). The average RMSE value at the vertical (elevation) dimension was 0.015 m and in the horizontal (spatial) dimension it was 0.02 m.

2.3.2 Estimation of wave hydrodynamics

The geometrical properties of the wave particularly the height of crest (H_c) and trough (H_t), breaking wave height (H_b), water depth (d), wavelength (L), surf zone width (W), run-up length of swash (L_s) and backwash (L_b), wave period (T) and frequency (f), angle of wave approach (α), wind speed (W_C) and direction were measured from the field. The average wave height (H), wave amplitude (a), and water depth (d) were measured as $H = H_c - H_t$, $a = H/2$, and $d = (H_c + H_t)/2$, respectively. The relative wave height at breaking was also measured as H_b/d . In this study, the on-field data of wave parameters were also validated by the instant results of the equation derived measurement. In this regard, the 'L' and 'f' were estimated by the equation of $L = T(gd)^{0.5}$ and $f = 1/T$, respectively. The RMSE of the observed data and equation-based results of 'L' are varied within 0.25–0.35 m. Moreover, the wave height and wave period were validated (through RMSE) with the Indian National Centre for Ocean Information Services (INCOIS) station data of the wave rider buoy (installed about 40 km east from the shoreline) in the Digha, which are significantly acceptable with RMSE of 0.05 m (wave height) and 0.12 s (wave period).

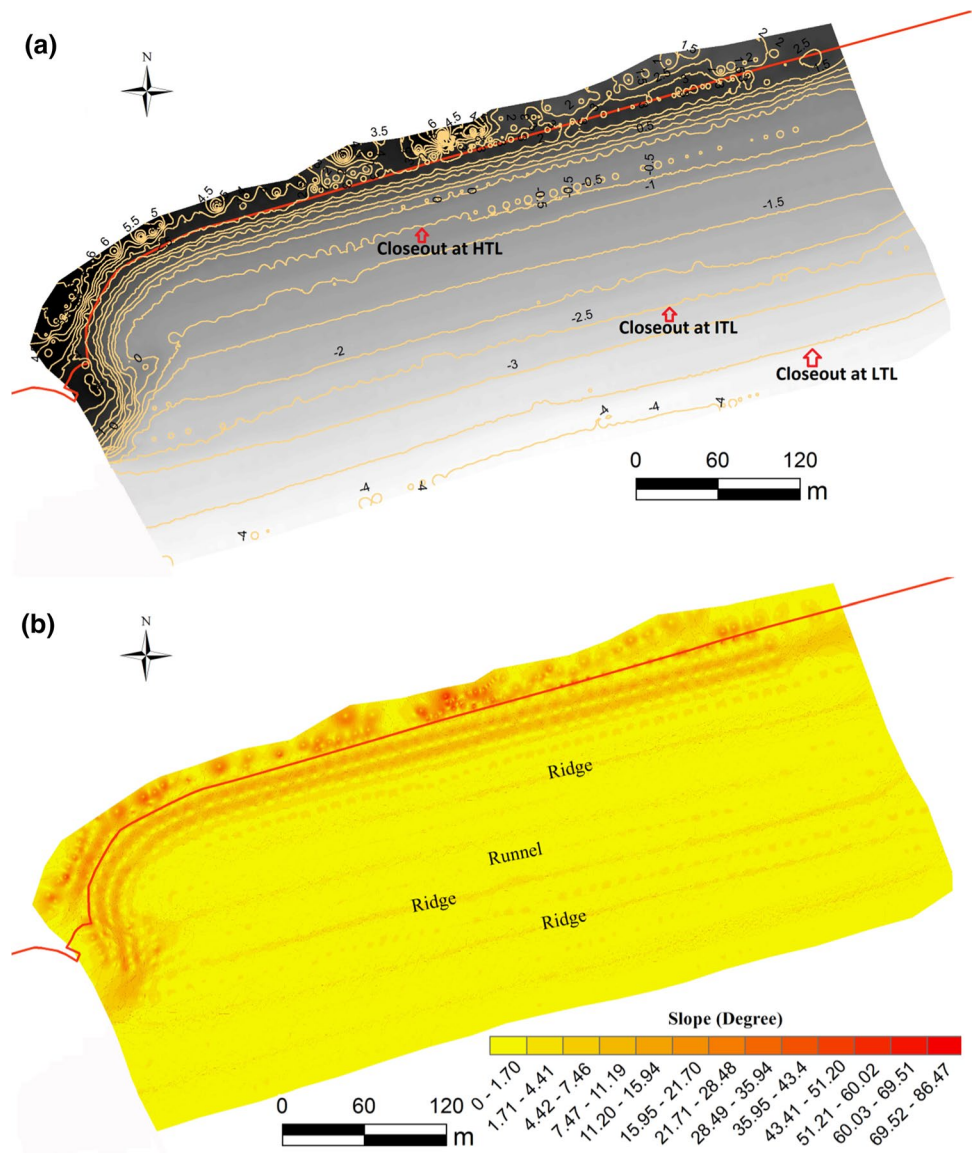
The wave geometry is understood from the ratios of relative water depth (d/L), relative wave height (H/d), and wave steepness during breaking (H/L), which describes the deep water ($d/L > 0.5$), transitional water ($0.1 < d/L < 0.5$) and shallow water ($d/L < 0.1$) environment. In this study, considering the shallow water environment, the equations were adopted to estimate the wave hydraulic parameters i.e. the wave phase velocity (C), wave crest velocity (C_b) (Van Dorn, 1978), wave energy (E), energy flux for each unit of wave crest (EC_n), breaking coefficient (h_b), and surf-scaling factor (ϵ) followed by Eqs. 1, 2, 3, 4, 5 and 6 (Guza & Inman, 1975), respectively.

$$C = (gd)^{0.5}, \quad (1)$$

$$C_b = (2gH_b)^{0.5}, \quad (2)$$

$$E = 1/8\rho gH^2, \quad (3)$$

Fig. 3 DEM-based (a) contour pattern of 0.5 m interval within the beach-dune premises indicating the depth of closure (closeout) at low tide level (LTL), intermediate tide level (ITL) and High tide level (HTL) in different beach elevation; and (b) the variation of slope shows the discriminate positions of ridge and runnel at a relatively higher and gentle slope, respectively



$$ECn = 0.5\rho g(H/2)^2(gd)^{0.5}, \tag{4}$$

$$h_b = (H/L) \tan^2 \beta, \tag{5}$$

$$\varepsilon = a_b \omega^2 / g \tan^2 \beta, \tag{6}$$

where ‘g’ is the gravitational acceleration (9.81 m/s²), and water density (ρ) is estimated through laboratory analysis as ρ = m/v, when, ‘m’ is the mass of water and ‘v’ stands for volume of water. In addition, ‘a_b’ is the wave breaker amplitude (H_b/2), and ‘ω’ is the incident wave radian frequency (ω = 2π/T).

The water depth varies according to the fluctuation of tide level. The mean water level (MWL) was assessed in the three different zones after considering the average tide level.

The entrainment threshold of sediment particle is defined by the depth of closure. The depth of closure was estimated using Eqs. 7, 8 and 9 (Hallermeier, 1981) for the nearshore (d_i) and offshore region (d_i). In this study, d_i is estimated for the three distinct zones (zone 1, 2 and 3) as water depth varies according to the tide level.

$$d_i = 2.28H_e - 68.5(H_e^2/gT_s^2), \tag{7}$$

$$d_i = (\bar{H}_s - 0.3\sigma_s)\bar{T}_s(g/5000D)^{0.5}. \tag{8}$$

Equation 7 has been simplified as Eq. 9.

$$d_i = 2\bar{H}_s + 11\sigma_s, \tag{9}$$

where $H_e = \overline{H_s} + 5.6\sigma_s$, σ_s is the standard deviation of the mean significant wave height ($\overline{H_s}$), the mean wave period (T_s) associated with $\overline{H_s}$, and D is mean grain size in mm.

2.3.3 Analysis of beach sediment

The results of sediment weight (gm) retained by individual sieve were converted into weight percentage distribution for analysis in the GRADISTAT statistical programme to understand the depositional environments (Jana & Paul, 2020). The mean, median, mode, sorting, skewness and kurtosis of grain size distribution were assessed to understand the influences of wave energy and beach morphology on the distinct beach environment during the deposition of particles.

2.3.4 Reciprocations of beach morphology, hydrodynamics and sediment

The resultant datasets of beach morphology, hydraulic and sedimentary nature were analyzed through principal component analysis (PCA) to select the significant components for multiple linear regression (MLR) and canonical correlation analysis (CCA) to establish the correlation between the components. In this study, 13 different multi-dimensional components have been considered from the four different environmental factors i.e. morphological factors (Y_1): beach elevation (B_E), and beach slope (β); hydrological factors (Y_2): wavelength (L), wave period (T), wave height (H), breaking wave height (H_b), and surf zone width (W), net sediment volume of swash and backwash (S_{SB}); sedimentological factors (Y_3): mean grain size (M_G), sorting (σ_I), skewness (Sk_I), and kurtosis (K_G); and meteorological factor: wind speed (W_C). Depending on the regression coefficients of the 13 components the independent and dependent variables were selected for CCA. The CCA assists to evaluate the strength of overall relationships of components with canonical variables.

3 Results and discussions

3.1 Morphological diversities of beach

Beach elevation and slope are envisaged as a controlling factor of beach morphodynamics, hydrodynamics and sedimentation pattern. Concerning the mean sea level, the maximum elevation (9.23 m) is recorded at the degraded dune top and the minimum (-4.15 m) at the extreme low-tide zone (Fig. 1). The elevation varies from -4.51 to 3 m within about 250 m distance across the beach. The seaside guard-wall cum road ensue ~ 3.25 m elevation as per the bathymetry survey result which is similar to the estimated

benchmark. The contour pattern (0.5 m interval) suggests that the beach elevation and slope are gradually increasing towards the upper beach-face from the seaside beach, which is analogous to the piling of sediment towards the upper beach-face in conjunction with the wave approach. Closely spacing crenulated contours (> 0 m) (Fig. 3a) indicates the higher slope ($> 4^\circ$) in the concreted upper beach-face (Fig. 3b). The crenulated contours are morphological indicators of mixer-energy environment dominated in the different ridge positions. The micro-level beach slope illustrates the existence of the relatively higher and lower slope along the ridge and runnel section, respectively in the middle-lower, middle and middle-upper beach sections (Figs. 3b, 4). The relatively steeper beach slope has been observed within -3 to -2 m contours (Fig. 3) which is formed by the deposition of sediment during the northeastern monsoon period (winter season). The relatively flat beach (between -2 and -1 m or -0.5 m contour) plays a pivotal role in maintaining the hydrodynamic behaviour and sedimentation pattern. In the upper beach-face (concreted erosion protecting structure combined with nine steps wave breakers), the high elevation (0 – 2 m) and slope ($> 4^\circ$) are responsible for high-energy wave breaking during extreme HTL. Among the 17 cross-profiles (P-1 to P-17), P-3 to P17 denotes a similar form of beach condition (Fig. 4). The P-1 prevails across the boulder-filled elevated wave protection structure and P-2 contiguous to it (Fig. 1). The -0.5 m and 0 m contour shows the prolonging cusps and horns along the upper beach-face (Fig. 5). The successive cusps and horns are almost equally spaced with an average length of 10 m and a width of 3.5 m, and elevation varies within 15–25 cm. These cups and horns are formed due to gradual erosion of sediment from the upper beach segment, which was deposited in the earlier winter season. From the geometrical point of view, other micro-morphological features (Fig. 6) are acutely placed within different beach sections. The swash marks (about 2.4–7.4 m length, 25–70 cm apart, and 3–6 cm height) are observed in the upper beach-face (Fig. 6a), ripples (~ 10 – 50 cm apart, and 0.5–2 cm height) in the middle beach zone (Fig. 6b), parallel ridge and runnel (Fig. 6c) remain along the beach stretch with an average spacing of 20 m and height ranging from 0.5 to 0.75 m.

3.2 Wave hydrodynamic variations

During the field investigation, the wind approached the coast from the S-SSE direction. The average wind speed varied within 0.97–3.16 m/s along with the recorded maximum (3.63 m/s) and minimum (0.50 m/s) speed (Table 1). The wave parameters are varied accordingly in three distinct zones in connection with beach morphological diversities. In zone 1 and 3, the wave height, water depth and wave period are correspondingly higher with the steeper beach slope. Due

Fig. 4 Cross-profiles along the seventeen transects between the edge of the surveyed area (towards the sea) and wave protecting guard-wall (landward side). Profiles are assembled through bathymetry survey (10 March 2018), which illustrates almost similar beach characteristics (except P1 and P2) all over the surveyed beach stretch comprising with ridge and runnel at different zones

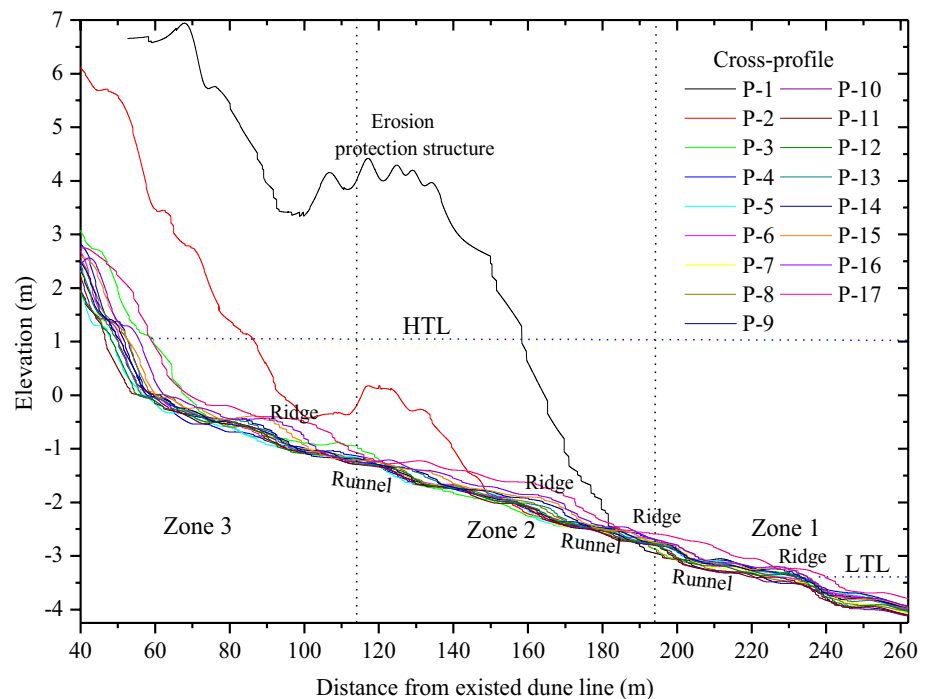
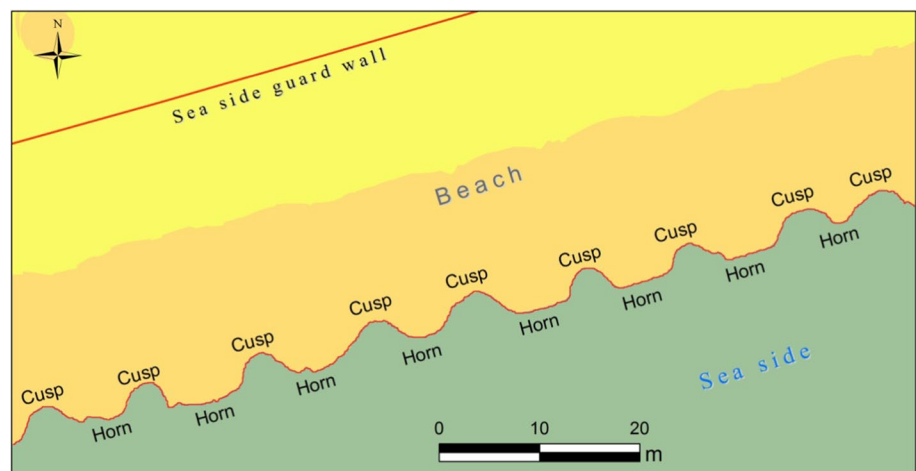


Fig. 5 Cusps and horns are fashioned along the 0 m contour (curved red line) at the upper beach-face in the eastern side of zone 3

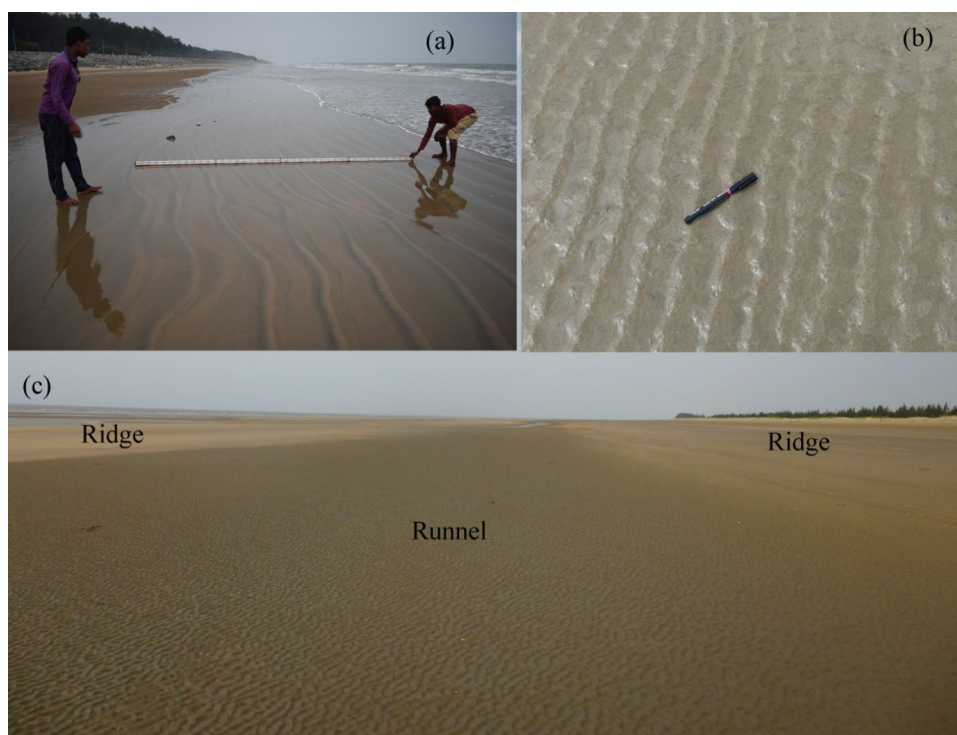


to the relatively gentle beach slope in zone 2 (Fig. 3), the wavelength and surf zone width are relatively greater in zone 2 in comparison to zone 1 and 3 (Table 1). However, based on the beach configuration, water depth and tide level, other parameter shows a discrepancy nature i.e. longshore/shore-normal current velocity is higher (~ 0.38 m/s) at LTL, and it gradually reduces towards upper beach-face (~ 0.18 m/s). Besides, the zone-wise maximum ($\sim 77.31^\circ$) and minimum ($\sim 72.43^\circ$) angle of wave approach are recorded in zone 2 and zone 1, respectively. Whereas, the moderate angle of wave approach ($\sim 73.99^\circ$) is observed in zone 3 due to a relatively steeper slope.

The relative water depth fluctuates between 0.075 and 0.124 m (Table 2). Such water depth indicates the

shallow water ($d/L < 0.1$) to transitional environment ($0.1 < d/L < 0.5$) (Carter, 2013). Wave energy and other wave hydrodynamic parameters (Table 2) are responsible for sediment entrainment, transport and deposition processes in different zones. In the shallow water environment, zones 1 and 3 experienced a relatively steeper beach slope in contrast to zone 2. Therefore, the wave energy parameter (Table 2) shows a relatively higher magnitude in zone 1 and 3 in comparison to zone 2. Moreover, depending on the tidal fluctuation, the depth of closure varies from 0.94 to 1.28 m in the different zones, whereas, the overall closeout is 1.34 m (Fig. 7; Table 3). The closeout depth is higher towards the offshore zone with its overall variation of 5.53–7.67 m (Table 3). The relative positions

Fig. 6 Various micro-landforms of (a) ripples, (b) swash-marks, and (c) ridge and runnel at the different beach segments



of the closeout change according to the LTL, intermediate tide level (ITL) and HTL (Fig. 3a). The closeout position remains in the relatively elevated beach segments in three different zones, and the sediment particles are trend to be entrained from these positions as per the tide levels.

Table 2 Comparisons of wave hydrodynamic components concerning the wave energy of different zones

Components	Zone 1	Zone 2	Zone 3
Water density (ρ) in Kg/m^3	1038	1038	1038
Relative depth of water (d/L)	0.124	0.075	0.121
Relative height of wave (H/d)	0.043	0.023	0.046
Wave velocity (C) in m/s	4.035	4.048	3.925
Wave steepness during breaking (H/L)	0.043	0.023	0.046
Relative wave height at breaking (H_b/d)	0.771	0.605	0.834
Wave frequency (f) per second	0.14	0.08	0.11
Wave crest velocity (C_b) in m/s	5.01	4.45	5.07
Angle of beach slope (β) in degree	1.219	0.984	1.534
Wave energy (E) in J/m^2	413.54	318.21	443.08
Energy flux for each unit of wave crest (EC_n) in k J/m^2	1.668	1.287	1.738
Breaking coefficient (h_b)	0.063	0.022	0.109
Surf scaling factor (ϵ)	0.034	0.025	0.038

3.3 Sedimentological variations

The sediment grain size characterization suggests that sediment particles are deposited in the intertidal zone under diverse hydrodynamic circumstances. The cumulative weight percentage distribution of 12 samples of set-3 (Fig. 8) illustrates the particle size distribution of different samples. S1, S5, S6 and S7 are dominated by very fine sand, whereas, S2, S3, S4 and S8 are composed of fine to very fine sand dominated by very fine sand. Also, four samples (S9–S12) are subjected to medium size sand with a little percentage of fine sand. The predomination of very fine sand in all sample sites reflects that the surface sediments are deposited under pleasant weather conditions without any storm effects. The statistical result of sediment analysis exhibits the mean, median, mode, sorting, skewness and kurtosis distribution of all 12 samples of set-3 (Table 4). The mean grain size varies from 3.102 to 1.723ϕ and the median of 3.197 – 1.602ϕ . The mean and median grain characterization indicates the very fine to medium size of sediment particles deposited in the surface with due effects from relatively firm to mixed-energy environment during the study period. The modal distribution shows (Table 4) the unimodal (S1 and S7), bimodal (S2, S3 and S6) and trimodal (S4, S5, and S8–S12) types of variations associated with the firm and mixed-energy environment. The samples of S1, S6 and S7 are well-sorted, whereas, S2–S5 and S9 are moderately well-sorted, and S8 and S10–S12 are moderately sorted (Table 4), which are also indicating the mixed-energy environment during sediment deposition. The skewness resulted as very fine

Fig. 7 Micro-zone wise sedimentation pattern and closeout depth in different tide condition in the nearshore part. The MWL of 1, 2 and 3 and overall MWL are placed based on the high and low water (tide) level of distinct zones during the study period

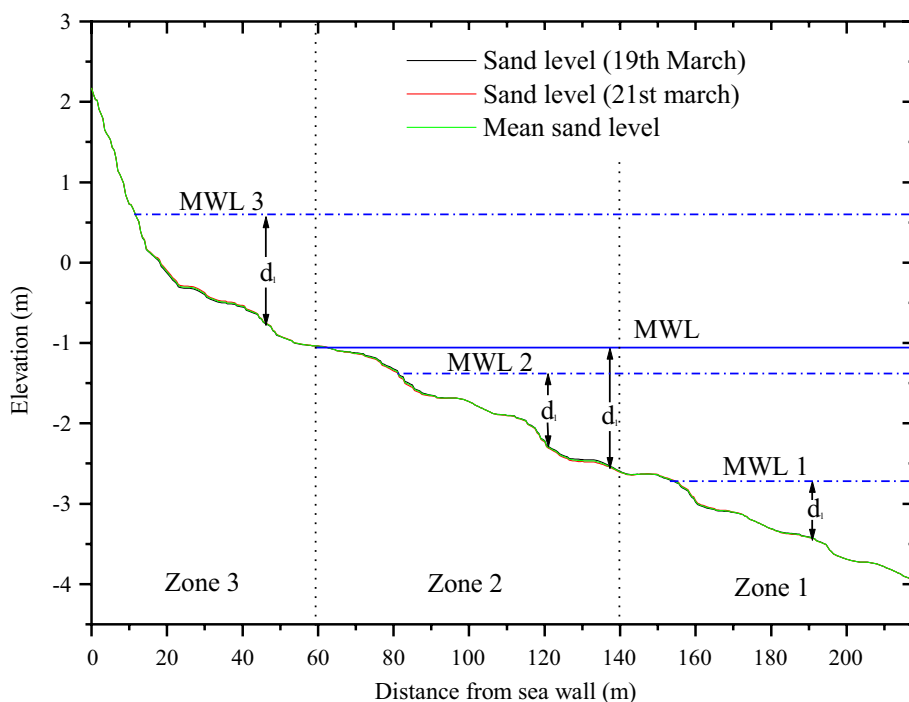


Table 3 Depth of closure in different tide conditions in three distinct beach zones

Zones	Tide condition	\bar{H}_s (m)	σ_s (m)	T_s (sec)	D (mm)	d_l (m)	d_f (m)
1	Low	0.25	0.071	8.33	0.144	1.28	7.65
2	Intermediate	0.21	0.047	9.53	0.115	0.94	7.67
3	High	0.37	0.030	4.97	0.200	1.07	5.62
Overall	MWL	0.23	0.080	7.72	0.162	1.34	5.53

Based on Eq. 9 ' d_l ' is estimated

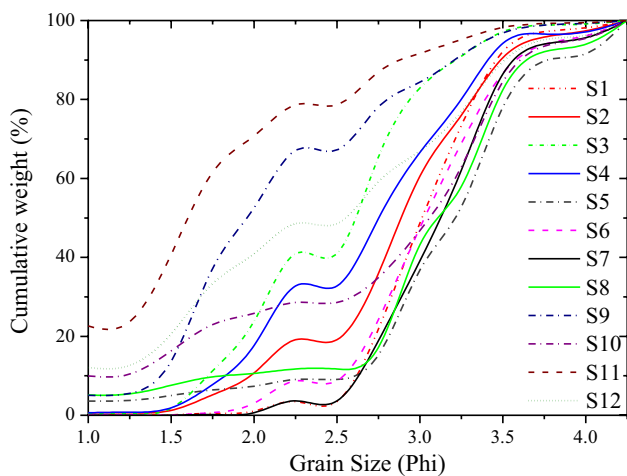


Fig. 8 The cumulative grain size distribution of twelve sediment samples of set-3

skewed (S8), fine skewed (S12), symmetrical (S1, S6 and S7), coarse skewed (S2 to S5, S9, S11 and S12) and very coarse skewed (S10) with overall variation from 0.041 to -0.204 . The positively skewed is associated with predominantly finer sediments under depositional environment, while, negative skewness indicates coarser sediments under high energy erosional environment (Pradhan et al., 2020). In addition, the kurtosis depicts the platykurtic (S3, S4, S10 and S12), mesokurtic (S1, S7 and S8), leptokurtic (S2, S6 and S11) and very leptokurtic (S5 and S9) type of distribution among 12 samples. The kurtosis provides the condition of fluctuating energy levels (Jana & Paul, 2020). In accordance with set-3, a similar type of grain size distribution is observed in other samples of set-1, 2 and 4 along the cross-profiles of CP-1, 2 and 4 (Fig. 1), respectively.

3.4 Interaction between beach morphology, hydrodynamics and sedimentology

The micro-level beach morphological diversities are investigated depending on the interaction between the beach morphodynamics, hydrodynamic and sedimentological

Table 4 Statistically described the nature of twelve sediment samples of set-3 along cross-profile 11 (P-11 or CP-3) within three beach zones

Analysis	Parameters											
	S1	S2	S3	S4	S5	S6	S7	S8	S9	S10	S11	S12
Numeric (\emptyset)	Mean	2.801	2.480	2.666	3.184	3.021	3.083	2.152	3.102	2.665	1.723	2.408
	Median	2.887	2.571	2.739	3.197	3.028	3.113	1.956	3.109	3.047	1.602	2.510
	Mode 1	2.868	2.605	2.605	3.356	3.119	3.356	1.616	3.356	3.356	0.868	3.356
	Mode 2	2.119	2.119	2.119	2.868	2.119	-	2.119	2.868	2.868	0.868	1.616
	Mode 3	-	-	-	3.356	4.200	-	-	2.605	0.868	1.616	2.605
Sorting	0.350	0.603	0.574	0.631	0.620	0.479	0.402	0.730	0.674	0.961	0.798	0.943
Skewness	0.041	-0.196	-0.162	-0.158	-0.161	-0.045	0.001	0.302	-0.204	-0.500	0.273	-0.152
Kurtosis	0.944	1.230	0.861	0.770	1.857	1.268	1.044	0.935	2.143	0.868	1.139	0.732
Descriptive	Very fine sand	Fine sand	Fine sand	Fine sand	Very fine sand	Very fine sand	Very fine sand	Fine sand	Very fine sand	Fine sand	Medium sand	Fine sand
Mode	Unimodal	Bimodal	Bimodal	Trimodal	Trimodal	Bimodal	Unimodal	Trimodal	Trimodal	Trimodal	Trimodal	Trimodal
Sorting	Well-sorted	Moderately well-sorted	Moderately well-sorted	Moderately well-sorted	Moderately well-sorted	Well-sorted	Well-sorted	Moderately sorted	Moderately well-sorted	Moderately sorted	Moderately sorted	Moderately sorted
Skewness	Symmetrical	Coarse skewed	Coarse skewed	Coarse skewed	Coarse skewed	Symmetrical	Symmetrical	Very fine skewed	Coarse skewed	Very coarse skewed	Fine skewed	Coarse skewed
Kurtosis	Mesokurtic	Leptokurtic	Platykurtic	Platykurtic	Very leptokurtic	Leptokurtic	Mesokurtic	Mesokurtic	Very leptokurtic	Platykurtic	Leptokurtic	Platykurtic

The analysis was done after Folk and Ward (1957). Sedimentary analysis of the other three sets of sediment samples (set-1, 2 and 4) have also resulted in a similar type of grain size distribution

variables. In zone 1, the beach elevation ranges between -4.15 and -2 m which gradually increase towards the upper beach section of zone 2. The moderate surf zone width (~ 66.55 m) and water depth (~ 1.62 m) vary according to the tide level in the relatively higher beach slope (1.68°) in zone 1. The depth of closure (1.28 m) ensures sediment entrainment around -3.5 m beach elevation at LTL in this zone. However, at the ITL, the depth of closure (0.94 m) exists around -2.5 m elevation in the transition zone of 1 and 2 due to moderate beach elevation (-2 to -0.5 m) and gentle beach slope (0.49° to 1.02°) in zone 2. Zone 3 is composed of relatively higher beach elevation (-0.015 to 1.15 m) and slope (1.2° – 2.15°). In this zone (around -0.5 m elevation), the depth of closure (1.07 m) ensures sediment entrainment at HTL. The moderate slope is responsible for high ' W ' (~ 85 m), whereas, the higher slope is responsible for a minimum ' W ' (~ 49.91 m). In such diverse circumstances, all the hydrological and sedimentological components are sensibly correlated (either positive or negative) with these three morphological and hydrological components (B_E , β and W).

The result of 13 component-based MLR analysis shows that the ' L ' and ' T ' are negatively correlated (-0.11 to -0.98) with ' B_E ' and ' β ', whereas, reverse (0.72 – 0.97) with the ' W '. The ' H ' and ' H_b ' are positively correlated (within 0.12 to 0.96) with the ' B_E ' and ' β ', whereas, negatively correlated with ' W ' (-0.69 to -0.94). This resultant correlation indicates the normal behaviour of the hydrodynamic mechanism in a constant meteorological condition. The sedimentological variables significantly react to the beach morphological variables. The ' S_{SB} ' is positively correlated with ' B_E ' (0.91 and 0.82) and ' β ' (0.15 and 0.88) in zone 1 and 3, respectively, whereas, in zone 2, it is inversely correlated with ' B_E ' (-0.30) and ' β ' (-0.29). The relatively higher elevation and slope are responsible for high-energy wave breaking and sediment entrainment in zone 1 and 3, which leads to the relatively greater volume of sediment transport as well as deposition towards the upper reaches of the respective zones. However, in the moderate beach elevation and slope in zone 2, the entrained sediments are not able to reach towards the upper reaches of zone 2 as the depth of closure remains in the transitional position of zone 1 and 2, and ' S_{SB} ' resulted in a deficit volume. The correlation of ' M_G ' (ϕ) with ' B_E ' and ' β ' shows a negative correlation as coarser particles tend to be deposited in the higher portion and settled down in the deeper portion of the beach following the greater wave energy factor and turbulence, respectively. The results of sediment sorting, skewness and kurtosis are the indicators of various wave energy environments during the deposition of sediment particles. The higher values of sorting (very well sorting) indicates the assemblage of different types of sediment particles associated with the mixed-energy environment,

while lower sorting values (very poorly sorted) depicts a uniform type of sediment grains resulted from steady energy (continuous high or low) environment (Inman & Chamberlain, 1955; Jana & Paul, 2020). The coarse (positive) skewed reveals either of depositional environment or superiority of finer particles, and fine (negative) skewed deals with either of the erosional condition associated with high energy environment or dominance of coarse particles (Pradhan et al., 2020). The flatness and peakedness trends both in sediment distribution and energy environment are reflected by the nature of kurtosis, it is less effective to explain erosion or accretion nature (Friedman, 1961; Pradhan et al., 2020). The sediment sorting and skewness are negatively correlated with ' M_G ', while, kurtosis is positively correlated with ' M_G ' (Fig. 9). The composition of sediment grain size in three different zones is described by the wave hydrodynamics and resultant energy level. In zone 1, the wave height, wavelength, surf zone width and wave period are moderate, coupled with the highest water depth, longshore current velocity and minimum angle of wave approach (Table 1). Also, the wave energy parameters remain moderate in zone 1 among the three distinct zones (Table 2). A nearly similar type of wave geometric and energy parameters was observed in zone 3, which mostly resulted in the higher value (except L , d , W , T , α and longshore current velocity) (Tables 1, 2). Such type of energetic hydrodynamic nature is responsible for sediment entrainment and transport according to the tidal fluctuation and depth of closure. In zone 2, all resultant parameters (Tables 1, 2) react as a neutral factor for sediment movement. Table 3 depicts the depth of closure (for nearshore zone and offshore region) at distinct zones with diverse hydrodynamic and sedimentary environments. In the nearshore zone, the resulted closeout depth (Table 3) varies according to the high, moderate and low hydrodynamic conditions respectively at zone 3, 1 and 2 (Tables 1, 2). The mean significant wave height and mean wave period are the significant factors to determine the closeout depth, which varies according to the tidal fluctuations (LTL, ITL and HTL), water depth, elevation, slope and wind speed. The mean grain size is also an important aspect determining the closeout depth. In zone 1, the highest depth of closure (1.28 m) resulted in the low-tide condition (Table 3). Whereas, the moderate (1.07 m) and low (0.94 m) closeout depth is observed correspondingly in zone 3 and 2. The overall depth of closure is 1.34 m within the entire beach stretch. The closeout depth in the offshore region is also significant for the sediment transport from the offshore region to the nearshore zone in association with longshore drift and littoral cell circulation. Figure 10 depicts very negligible erosion and mostly stable beach condition in the extreme seaward position of the studied beach stretch, while, meager deposition over the lower beach ridge

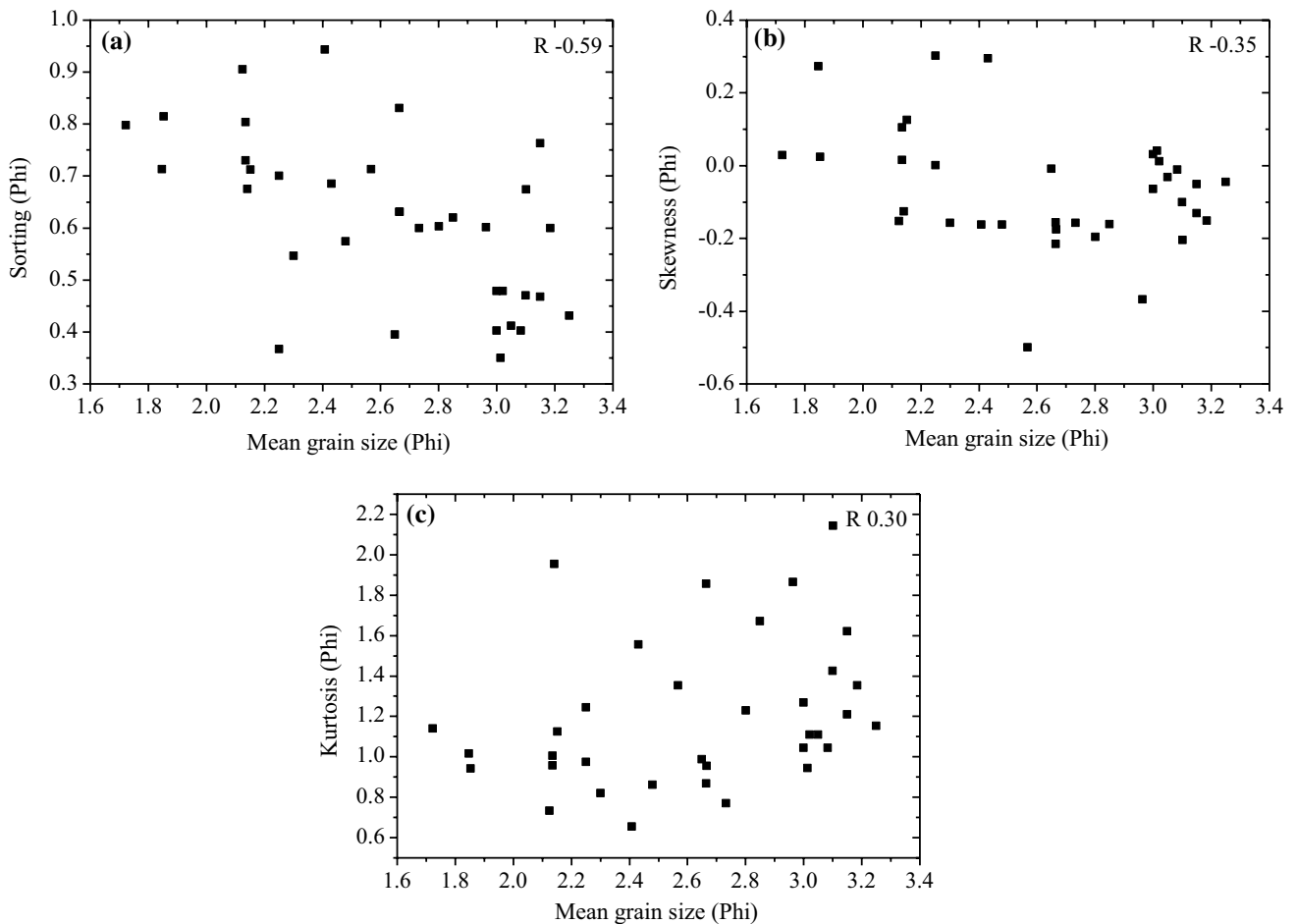


Fig. 9 The respective relationship between mean grain size and (a) sorting, (b) skewness, and (c) kurtosis of entire (48) sediment samples

section (just near the LTL). In the upper beach-face higher rate of sediment deposition is observed due to sediment supply from the erosive middle beach section of zone 2. In this zone, the scouring effect is responsible for such erosion during wave and tidal actions within higher surf zone width. Therefore, during the study period, some shallow scouring pools were observed in the middle beach section. The hydraulic energy level and sedimentation patterns are responsible for the formation of various micro-morphological features across the beach. Likewise, the cusps and horns have been formed in the upper beach-face due to sedimentation in high-energy conditions. However, during the full-moon and new-moon phases, the deposited sediments are removed from the upper beach-face due to the very high energetic backward movement of water through the concreted steeper erosion protective structures. Such kind of sediment removal intensified during the storm surge events, and the toe-erosion accelerates at the bottom of the concreted erosion protection structures. Relatively elevated and closely interspaced ripples have been observed at the middle beach section (zone 2) resulted

from the spilling wave breaking and scouring effects. The swash marks are observed particularly along the transition zone of the upper beach-face and middle beach section, where relatively steeper beach surface allowed backwash to return at higher velocities.

The CCA was done based on Eigen values, variability and cumulative variability of four canonical factors (F_1 , F_2 , F_3 and F_4) (Table 5). The F_1 and F_2 includes 85.544% of the total variance (Table 5), and these two CCA factors are considered for correlation analysis. The CCA shows the consistency of different factors concerning the selected components of four different environmental factors (Y_1 , Y_2 , Y_3 and Y_4). Correlation between the dependent and canonical variables (Table 6) illustrate that ' L ', ' T ', ' M_G ', ' Sk_I ' and ' K_G ' are positively correlated, and ' H ', ' H_b ', ' S_{SB} ' and ' σ_I ' are negatively correlated with F_1 . Similarly, the correlation between the dependent variables and F_2 , F_3 and F_4 are represented in Table 6, however, correlations of F_1 and F_2 are considered on the basis of those CCA factors ensure more than 0.90 of canonical correlation (Table 5). The five environmental factors of dependent and independent

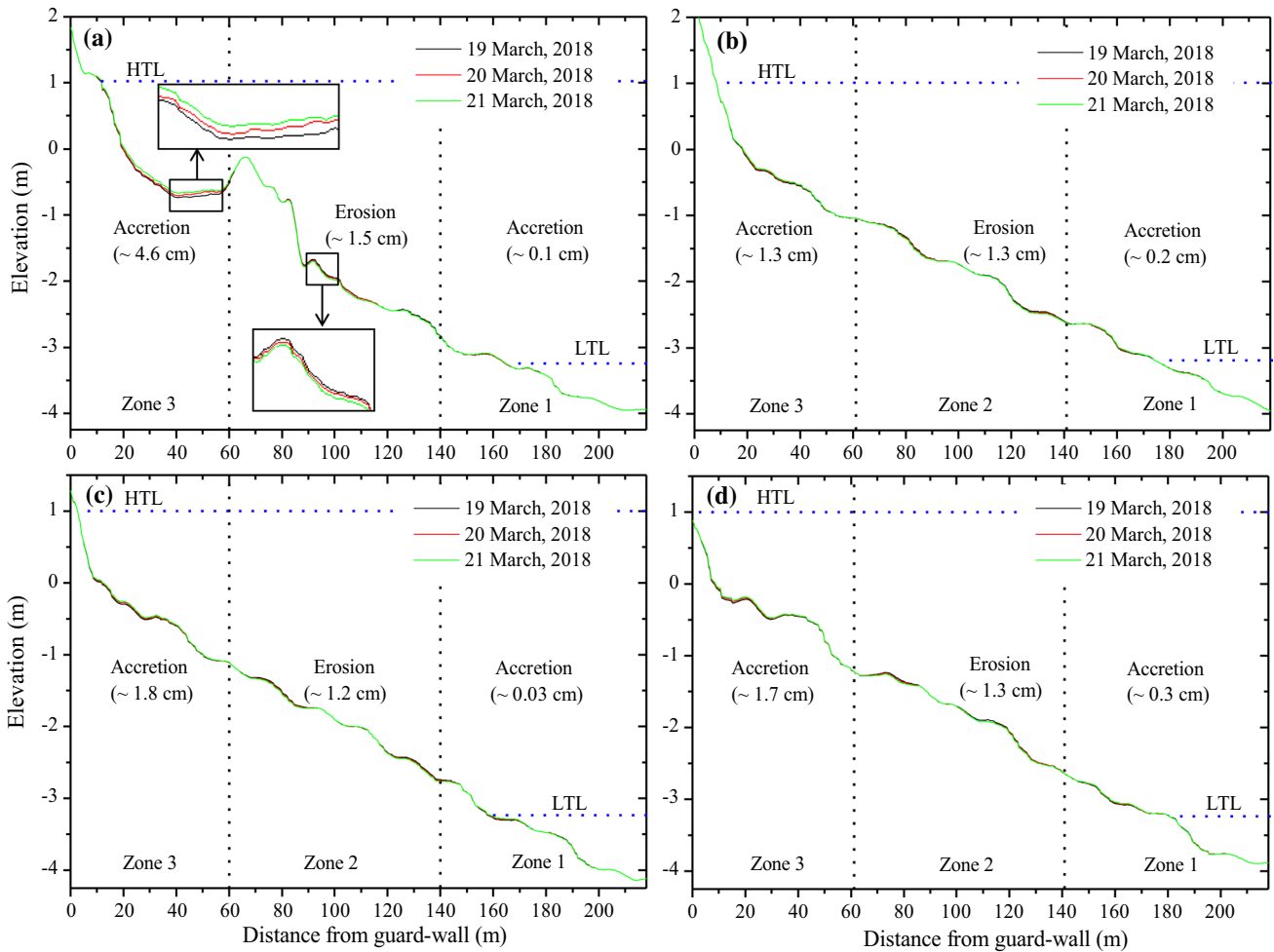


Fig. 10 Cross-profiles of consecutive three days survey along the four selected transects (CP-1 to 4) depicts the sediment erosion and accretion positions. The average net thickness of sediment accretion

is estimated as (a) 0.81 cm, (c) 0.11 cm, and (d) 0.14 cm along the CP-1, CP-2 and CP-4, respectively, and (b) erosion of 0.02 cm along the CP-3

Table 5 Eigenvalue and canonical correlations

CCA factors	Eigen value	Variability (%)	Cumulative variability (%)	Canonical correlation
F_1	0.843	55.631	55.631	0.99
F_2	0.414	28.913	85.544	0.91
F_3	0.210	12.227	97.771	0.81
F_4	0.116	3.229	100.000	0.48

variables are somehow manifest with positive or negative correlation with the canonical variables of F_1 and F_2 (Table 6). Among the hydrological components, ' L ' and ' H_b ' confirm a positive correlation, while, ' T ', ' H ' and ' S_{SB} ' resulted in negative correlation. Besides, it is observed that ' T ' is anti-correlated with ' H_b ', and ' H ' and ' S_{SB} ' are anti-correlated with ' L '. Such anti-correlation

suggests that ' T ' is less when ' H_b ' is high, and ' H ' and ' S_{SB} ' are less when ' L ' is high. It clearly indicates that ' T ', ' H ' and ' S_{SB} ' reduces with increasing of ' H_b ' and ' L ' at both sides of the elevated and steeper beach ridge positions. Moreover, sedimentological factors indicate the positive correlation of ' Sk_I ', and ' M_G ', ' σ_I ' and ' K_G ' are manifest a negative correlation, while, ' σ_I ' is anti-correlated with ' Sk_I '. This indicates that ' σ_I ' is less when ' Sk_I ' is high. It is due to the dominance of deposition by finer sediments in the steady energy environment, and less area is conveyed with mixed-energy environment associated with less ' σ_I '. Moreover, both the morphological components ' B_E ' and ' β ', and hydrological component ' W ' shows the positive correlation, while, meteorological component reveals the negative correlation with the canonical variables of F_1 and F_2 . The components having positive correlations ensure a significant role in the beach sedimentation process.

Table 6 Correlations between dependent and independent variables with canonical variables

Variables	Environmental factors	Components	Canonical variables			
			F_1	F_2	F_3	F_4
Dependent	Hydrological	Wavelength (L)	0.64	0.50	-0.29	0.18
		Wave period (T)	0.98	-0.04	0.12	-0.04
		Wave height (H)	-0.90	-0.15	0.28	-0.007
		Breaking wave height (H_b)	-0.99	0.01	0.07	-0.02
		Sediment volume of swash-backwash (S_{SB})	-0.81	-0.53	-0.07	0.11
	Sedimentological	Mean grain size (M_G)	0.66	-0.34	0.15	0.32
		Sorting (σ_I)	-0.81	-0.12	-0.38	0.02
		Skewness (Sk_I)	0.15	0.30	-0.19	-0.58
		Kurtosis (K_G)	0.12	-0.32	-0.42	-0.31
		Independent	Morphological	Beach elevation (B_E)	-0.33	0.40
Beach slope (β)	-0.98			0.83	0.20	0.02
Hydrological	Surf zone width (W)		0.82	0.40	-0.25	0.32
Meteorological	Wind speed (W_C)		-0.75	-0.52	0.12	0.39

3.5 Interacting response on beach morphology

The results of sedimentological analysis and interaction between different variables are intimate to understand the beach morphological diversities and sedimentation pattern. Only 17% of the total (48) samples are collected beyond the extreme LTL. The statistical result of these samples reveals unimodal, very fine sand, well-sorted, symmetrical skewed and mesokurtic type of distribution (Table 4). Such a type of sedimentary deposits indicates a low-energy environment at the stretch of extreme LTL. Moreover, most of the samples (25%) have resulted with medium–fine sand, which is deposited under a relatively high-energy environment (Table 2) which is analogous to relatively high beach elevation and steep slope in the distinctive zones. In the upper part of zone 1, the trimodal (15%), and leptokurtic (6%) to very leptokurtic (10%) types of sedimentary nature (Table 4) reveals the mixed high-energy environment caused by high-energy wave breaking during rising and falling tides over the relatively elevated and steeper ridge top. In zone 2, extremely symmetrical and moderate energy level (Table 2) is responsible for unimodal to bimodal type of sedimentation. Moreover, in zone 2, 25% samples are significantly characterized by very fine sand, well-sorted, symmetrical skewed, and mesokurtic, whereas, 8% samples remain under fine sand, moderately sorted, very fine skewed, and leptokurtic type of sedimentary distribution (Table 4). All those sediments are deposited in the relatively firm and moderate wave energy environment (Table 2) associated with relatively flat beach status (moderate elevation and gentle slope). The symmetrical wave energy environment is responsible for the formation of ripples in the middle section of zone 2 (Fig. 6b). The scouring pools are formed in the transitional zones (in-between zone 1 and 2, and 2 and 3) due to the mixed high-energy

environment at the shallow water depth. This mixed high-energy environment is further validated with the trimodal types of sedimentary nature (Table 4). The very fine (4%), fine (8%), and medium (12%) grain sand is observed, respectively in the lower, middle and upper parts of zone 3 which indicates the gradual increase of energy level towards the upper beach-face. Significantly, all sediment samples classified in this zone are trimodal and moderately sorted. Such kind of sedimentary distribution confers a gradual increasing nature of mixed high-energy environment towards zone 3 from zone 1 and 2. Fine (4%) to very coarse skewed (8%) with the dominance of coarse skewed (13%) sediment indicates the alteration of energy level during rising and falling tide conditions at the extreme high-tide stage. All these sedimentary nature indicates an escalating trend of energy level towards the upper beach-face of zone 3 succeeding zone 1

Table 7 Compendium of net sediment volume per successive swash and backwash after three events

Zone	Variable	Net sediment volume (gm)	Sedimentation nature
1	Maximum	+155.02	Accretion
	Minimum	-19.16	
	Average	+50.09	
2	Maximum	+123.34	Erosion
	Minimum	-185.14	
	Average	-52.62	
3	Maximum	+212.26	Accretion
	Minimum	+75.41	
	Average	+132.36	

The sediment surplus or accretion is indicated by '+' as the volume of sediment arrested in swash is > backwash, and deficit or erosion (-) is the mirror of accretion

and 2 (Table 2). In the upper beach-face the regular spacing cusps and horns are fashioned with the fine to a very coarse skewed type of sedimentation in response to mixed high (rising tide) and low (falling tide) energy environments. The swash marks are shaped by steady-state energy conditions in the steeper beach slope of the upper beach-face due to maximum swash and backwash run-up velocity.

3.6 Short-term sedimentation pattern

The net sediment volume of swash and backwash waves in three different zones (Table 7) reveals the nature of sediment deposition in zone 1 and 3, and erosion in zone 2. In this context, the average net volume of sediment accretion (50.09 gm) in zone 1 is virtually identical with sediment erosion (−52.62 gm) from zone 2. But, at zone 3, a higher volume (~132.36 gm) of net sediment accumulation (Table 7) confers the sediment accretion within 3 days (Table 8). The sedimentary nature and depositional environments reveal that the least volume of sediment deposited in the upper part of zone 1, and greater volume of sediment deposited in the upper beach-face of zone 3, while, the relatively scanty amount of sediment eroded from zone 2 (Fig. 10; Table 8). Moreover, in zone 2, the nature of sediment characteristics and scouring in the mixed-energy

environment is responsible for sediment erosion. However, the higher volume of sediment deposited (accretion) in zone 3, which can be transported by the longshore current and littoral cell circulation systems from the estuarine part of the Subarnarekha river (beyond the studied beach section) (Maiti & Bhattacharya, 2009). Also, an inadequate amount of sand (eroded from zone 2) is deposited in zone 3. The earlier studies by Maiti and Bhattacharya (2009, 2011), Jana and Bhattacharya (2013) and Jana et al. (2014) suggest a significant trend of shoreline erosion (−19.98 m/y) during 1972–2010 in this stretch, which indicates an extreme erosive nature based on Luijendijk et al. (2018). Besides, the seasonal sedimentation (erosion and accretion) pattern during the post-monsoon (December 2008) and pre-monsoon (April 2009) period shown the 24.042 m³ volume of sediment erosion (Adhikari et al., 2016). However, in this study, the composite beach profile shows more sediment deposition at the eastern part of the study area in comparison to the western part (Fig. 10; Table 8). The estimated average net thickness of sediment accretion and erosion along every profile (CP-1 to 4) endorses the accretion in zone 1 and 3, while, erosion in zone 2 (Fig. 10; Table 8). During the study period, along CP-1, the maximum accretion (8 cm) and erosion (−3.7 cm) were recorded in zone 3 and 2 (Table 8), respectively (Fig. 10a). The higher accretion takes place in the pocket section on erosion protection structure in zone 3, whereas, erosion intensifies at the seaward side of the erosion protection structure (zone 2). In the other profiles, the overall accretion and erosion vary between 3.8–3.1 cm (maximum) and 3.3–3.0 cm (minimum), respectively (Table 8). The overall higher accretion is found within −0.01 m to −0.05 m elevation of zone 3 (at 10–40 m beach width from the concrete fence) (Fig. 3).

Table 8 Nature of sedimentation within three days on 19 – 21 March 2020 (at Waxing Crescent phase) along the four distinct cross-profiles in three diverse beach zones

Cross-profile	Zone	Thickness of sedimentation accretion / erosion (cm)			Average sedimentation nature
		Maximum	Minimum	Average	
CP-1	1	+1.30	−1.30	+0.07	Accretion
	2	+0.12	−3.70	−1.52	Erosion
	3	+8.00	0.00	+4.57	Accretion
	Overall	+8.00	−3.70	+0.81	Accretion
CP-2	1	+2.10	−1.50	+0.18	Accretion
	2	+0.30	−3.00	−1.33	Erosion
	3	+3.10	0.00	+1.30	Accretion
	Overall	+3.10	−3.00	−0.02	Erosion
CP-3	1	+2.20	−2.60	+0.02	Accretion
	2	+0.50	−3.10	−1.20	Erosion
	3	+3.60	0.00	+1.81	Accretion
	Overall	+3.60	−3.10	+0.11	Accretion
CP-4	1	+2.02	−0.90	+0.30	Accretion
	2	+0.03	−3.30	−1.33	Erosion
	3	+3.80	+0.13	+1.72	Accretion
	Overall	+3.80	−3.30	+0.14	Accretion

Accretion (+) and erosion (−) are estimated depending on the elevation difference between the higher and lower positions at each station (0.5 m interval) of three days composite profiles

4 Conclusions

Generally, seasonal and long-term sedimentation and beach morphological studies have been carried out on different beach stretches throughout the globe, which is easy enough to recognize the controlling processes and morphological changes and their impacts on the beach environment. The beach erosion is associated with the monsoonal disturbances, whereas, gradual accretion is observed during post- and pre-monsoon periods in the tropical monsoon-dominated coasts. Meanwhile, the assessment of morphological and sedimentological adjustments in association with the hydrodynamic processes during calm weather conditions was neglected for insignificant or negligible changes in beach form regulated by erosion and accretion nature. Moreover, the beach nourishment and management plans have been adopted only considering the high magnitude monsoonal devastation without prior consideration of the natural hydrodynamic processes

throughout the year or in calm weather conditions. However, the present study reveals that the beach sedimentation pattern and morphological forms have been changed with the hydrodynamic behaviour in an association of fluctuating tide levels. During the last 2 or 3 decades, the concreted or hard erosion protection structures have been constructed on the Digha coast at the cost of huge investment. However, these preventive measures somehow can only be able to protect lateral erosion but exaggerates the vertical erosion (mainly in the form of toe-erosion) as well as beach lowering. Therefore, the soft management plan is to be implemented instead of hard defense structures to reduce beach erosion by arresting the accreted sediment in the upper beach-face. Hence, such kind of study can be useful for decision-making towards the soft nourishment strategies despite the hard engineering structures in the nearshore areas. Therefore, the present study has paramount importance for other similar sandy beaches, particularly in the coastal areas of the tropical monsoon climate region.

Acknowledgements The author would like to thank Mr. Abhijit Gayen, Ms. Nandini Jana, Mrs. Kalyani Das and Mr. Umesh Bera and other M.Sc. students of session 2016–2018, Department of Geography, Bajkul Milani Mahavidyalaya for their efficient support during the period of intensive fieldwork. The valuable comments and suggestions from the anonymous reviewers on the different aspects of the manuscript are highly acknowledged.

Data availability statement All tables and figures used in the submitted article were generated during the study period which can be available from the author on reasonable request.

References

- Adhikari, M. D., Maiti, S., Patra, S., Jana, A., Maiti, S. K., & Sengupta, A. (2016). GIS based beach sand budget analysis through seasonal beach profiling using cartographic techniques. *Modeling Earth Systems and Environment*, 2(2), 74.
- Ariffin, E. H., Sedrati, M., Akhir, M. F., Norzilah, M. N. M., Yaacob, R., & Husain, M. L. (2019). Short-term observations of beach Morphodynamics during seasonal monsoons: Two examples from Kuala Terengganu coast (Malaysia). *Journal of Coastal Conservation*, 23(6), 985–994.
- Belliard, J. P., Silinski, A., Meire, D., Kolokythas, G., Levy, Y., Van Braeckel, A., et al. (2019). High-resolution bed level changes in relation to tidal and wave forcing on a narrow fringing macrotidal flat: Bridging intra-tidal, daily and seasonal sediment dynamics. *Marine Geology*, 412, 123–138.
- Bhattacharya, A., Sarkar, S. K., & Bhattacharya, A. (2003). An assessment of coastal modification in the low lying tropical coast of north east India and role of natural and artificial forcings. *Proceedings of International Conference on Estuaries and Coasts*, 9, 158–165.
- Birkemeier, W. A. (1985). Field data on seaward limit of profile change. *Journal of Waterway, Port, Coastal, and Ocean Engineering*, 111(3), 598–602.
- Blatt, H., Middleton, G. V., & Murray, R. C. (1980). *Origin of sedimentary rocks* (2nd ed., p. 766). Prentice-Hall.
- Blott, S. J., & Pye, K. (2001). GRADISTAT: A grain size distribution and statistics package for the analysis of unconsolidated sediments. *Earth Surface Processes and Landforms*, 26(11), 1237–1248.
- Brinkkemper, J. A., Aagaard, T., De Bakker, A. T. M., & Ruessink, B. G. (2018). Shortwave sand transport in the shallow surf zone. *Journal of Geophysical Research: Earth Surface*, 123(5), 1145–1159.
- Butt, T., & Russell, P. (2000). Hydrodynamics and cross-shore sediment transport in the swash-zone of natural beaches: A review. *Journal of Coastal Research*, 16(2), 255–268.
- Carter, R. W. G. (2013). *Coastal environments: An introduction to the physical, ecological, and cultural systems of coastlines*. Elsevier.
- Chakrabarti, P. (1991). Process-response system analysis in the macrotidal estuarine and mesotidal coastal plain of eastern India. *Geological Society of India Memoir*, 22, 165–181.
- Chempalayil, S. P., Kumar, V. S., Dora, G. U., & Johnson, G. (2014). Near shore waves, long-shore currents and sediment transport along micro-tidal beaches, central west coast of India. *International Journal of Sediment Research*, 29(3), 402–413.
- Folk, R. L., & Ward, W. C. (1957). Brazos River bar: A study in the significance of grain size parameters. *Journal of Sedimentary Research*, 27(1), 3–26.
- Friedman, G. M. (1961). Distinction between dune, beach, and river sands from their textural characteristics. *Journal of Sedimentary Research*, 31(4), 514–529.
- Guza, R. T., & Inman, D. L. (1975). Edge waves and beach cusps. *Journal of Geophysical Research*, 80(21), 2997–3012.
- Hallermeier, R. J. (1981). A profile zonation for seasonal sand beaches from wave climate. *Coastal Engineering*, 4, 253–277.
- Inman, D.L., & Chamberlain, T.K. (1955). Particle-size distribution in nearshore sediments. In: Hough, J. L. and Menard, H. W. (Eds), *Finding Ancient Shorelines-Soc. Econ. Palaeontologists Mineralogists, Spec. Publ.*, 3 pp. 106–129.
- Jackson, N. L., Nordstrom, K. F., & Farrell, E. J. (2017). Longshore sediment transport and foreshore change in the swash zone of an estuarine beach. *Marine Geology*, 386, 88–97.
- Jana, A., & Bhattacharya, A. K. (2013). Assessment of coastal erosion vulnerability around Midnapur-Balasore Coast, Eastern India using integrated remote sensing and GIS techniques. *Journal of the Indian Society of Remote Sensing*, 41(3), 675–686.
- Jana, A., Biswas, A., Maiti, S., & Bhattacharya, A. K. (2014). Shoreline changes in response to sea level rise along Digha Coast, Eastern India: An analytical approach of remote sensing, GIS and statistical techniques. *Journal of Coastal Conservation*, 18(3), 145–155.
- Jana, S., & Paul, A. K. (2020). Chronological evolution of the channel functional units in association with palaeo-hydrogeomorphological environment in the ancient delta fan of Subarnarekha basin, India. *Environmental Earth Sciences*, 79(13), 1–24. <https://doi.org/10.1007/s12665-020-09093-1>
- Jayakumar, S., Raju, N. S. N., & Gowthaman, R. (2004). Beach dynamics of an open coast on the west coast of India. In: *3rd Indian national conference on Harbour & Ocean engineering*, NIO, Goa. pp. 9–16
- Jayappa, K. S., Kumar, G. V., & Subrahmanya, K. R. (2003). Influence of coastal structures on the beaches of southern Karnataka, India. *Journal of Coastal Research*, 19(2), 389–408.
- Joevivek, V., & Chandrasekar, N. (2019). Temporal Trends of Breaker Waves and Beach Morphodynamics Along the Central Tamil Nadu Coast, India. In *Coastal Zone Management*. Elsevier, pp. 207–229.
- Joevivek, V., Chandrasekar, N., Saravanan, S., Anandakumar, H., Thanushkodi, K., Suguna, N., & Jaya, J. (2018). Spatial and temporal correlation between beach and wave processes: implications for bar–berm sediment transition. *Frontiers of Earth Science*. <https://doi.org/10.1007/s11707-017-0655-y>

- Kaliraj, S., Chandrasekar, N., & Ramachandran, K. K. (2017). Mapping of coastal landforms and volumetric change analysis in the south west coast of Kanyakumari, South India using remote sensing and GIS techniques. *The Egyptian Journal of Remote Sensing and Space Science*, 20(2), 265–282.
- Komar, P. D. (2018). Beach processes and erosion—an introduction. In *Handbook of coastal processes and erosion*. CRC Press, 1–20.
- Laing, A. K. (1998). An introduction to ocean waves. *World Meteorological Organization. Guide to Wave Analysis and Forecasting. Second Edition. Switzerland: WMO - N° 702*, 1–14
- Luijendijk, A., Hagenaars, G., Ranasinghe, R., Baart, F., Donchyts, G., & Aarninkhof, S. (2018). The state of the world's beaches. *Scientific Reports*, 8(1), 1–11.
- Maiti, S., & Bhattacharya, A. K. (2009). Shoreline change analysis and its application to prediction: A remote sensing and statistics based approach. *Marine Geology*, 257, 11–23.
- Maiti, S., & Bhattacharya, A. K. (2011). A three-unit-based approach in coastal-change studies using Landsat images. *International Journal of Remote Sensing*, 32(1), 209–229.
- Masselink, G., Auger, N., Russell, P., & O'Hare, T. I. M. (2007). Short-term morphological change and sediment dynamics in the intertidal zone of a macrotidal beach. *Sedimentology*, 54(1), 39–53.
- Masselink, G., & Hegge, B. (1995). Morphodynamics of meso- and macrotidal beaches: Examples from central Queensland, Australia. *Marine Geology*, 129, 1–23.
- Masselink, G., & Short, A. D. (1993). The effect of tide range on beach morphodynamics and morphology: A conceptual beach model. *Journal of Coastal Research*, 9(3), 785–800.
- Mondal, D. (2021). Coastal urbanization and population pressure with related vulnerabilities and environmental conflicts a case study at Medinipur Littoral Tract West Bengal. Unpublished Ph.D thesis submitted to Vidyasagar University, Midnapore, West Bengal, India.
- Morang, A., & Birkemeier, W. A. (2005). Depth of closure on sandy coasts. In: Schwartz, M. L. (ed.), *Encyclopedia of Coastal Science*. Dordrecht, the Netherlands: Springer, pp. 374–376.
- Mujal-Colilles, A., Grifoll, M., & Falqués, A. (2019). Rhythmic morphology in a microtidal low-energy beach. *Geomorphology*, 334, 151–164.
- Patra, A., & Bhaskaran, P. K. (2017). Temporal variability in wind-wave climate and its validation with ESSO-NIOT wave atlas for the head Bay of Bengal. *Climate Dynamics*, 49(4), 1271–1288.
- Pradhan, U. K., Sahoo, R. K., Pradhan, S., Mohany, P. K., & Mishra, P. (2020). Textural analysis of coastal sediments along east coast of India. *Journal of the Geological Society of India*, 95(1), 67–74.
- Purkait, B., & Majumdar, D. D. (2014). Distinguishing different sedimentary facies in a deltaic system. *Sedimentary Geology*, 308, 53–62.
- Purkait, B., Majumdar, D. D., & Mazumder, R. (2017). Bed roughness and grain sorting—an experimental study over fine to medium sand beds. *International Journal of Sediment Research*, 32(3), 384–400.
- Ramakrishnan, R., Agrawal, R., Remya, P. G., NagaKumar, K. C. V., Demudu, G., Rajawat, A. S., et al. (2018). Modelling coastal erosion: A case study of Yarada beach near Visakhapatnam, east coast of India. *Ocean & Coastal Management*, 156, 239–248.
- Short, A. D., & Wright, L. D. (2018). Morphodynamics of beaches and surf zones in Australia. In *Handbook of coastal processes and erosion*, 35–64.
- Singh, O. P., Khan, T. M. A., & Rahman, M. S. (2001). Has the frequency of intense tropical cyclones increased in the north Indian Ocean? *Current Science*, 80(4), 575–580.
- Sreenivasulu, G., Jayaraju, N., Reddy, B. S. R., Prasad, T. L., Lakshmana, B., & Nagalakshmi, K. (2017). Coastal morphodynamics of Tupilipalem Coast, Andhra Pradesh, southeast coast of India. *Current Science*, 112(4), 823.
- Van Dorn, W. G. (1978). Breaking invariants in shoaling waves. *Journal of Geophysical Research: Oceans*, 83(C6), 2981–2988.
- Williams, A. T., Rangel-Buitrago, N., Pranzini, E., & Anfuso, G. (2018). The management of coastal erosion. *Ocean & Coastal Management*, 156, 4–20.
- Wright, L. D., & Short, A. D. (1984). Morphodynamic variability of surf zones and beaches: A synthesis. *Marine Geology*, 56, 93–118.

Publisher's Note Springer Nature remains neutral with regard to jurisdictional claims in published maps and institutional affiliations.